The Campi Flegrei caldera: unrest mechanisms and hazards

G. DE NATALE[1], C. TROISE[1], F. PINGUE[1], G. MASTROLORENZO[1],
L. PAPPALARDO[1], M. BATTAGLIA[2] & E. BOSCHI[1].

[1]*Istituto Nazionale di Geofisica e Vulcanologia, Via Diaclezano 328, 80124 Napoli, Italy
(e-mail: troise@ov.ingv.it)*

[2]*Department of Structural Geology & Geodynamics, University of Göttingen,
37077 Göttingen, Germany*

Abstract: In the last four decades, Campi Flegrei caldera has been the world's most active caldera characterized by intense unrest episodes involving huge ground deformation and seismicity, but, at the time of writing, has not culminated in an eruption. We present a careful review, with new analyses and interpretation, of all the data and recent research results. We deal with three main problems: the tentative reconstruction of the substructure; the modelling of unrest episodes to shed light on possible pre-eruptive scenarios; and the probabilistic estimation of the hazards from explosive pyroclastic products. The results show, for the first time at a volcano, that a very peculiar mechanism is generating episodes of unrest, involving mainly activation of the geothermal system from deeper magma reservoirs. The character and evolution of unrest episodes is strongly controlled by structural features, like the ring-fault system at the borders of the caldera collapse. The use of detailed volcanological, mathematical and statistical procedures also make it possible to obtain a detailed picture of eruptive hazards in the whole Neapolitan area. The complex behaviour of this caldera, involving interaction between magmatic and geothermal phenomena, sheds light on the dynamics of the most dangerous types of volcanoes in the world.

The Campi Flegrei volcanic field (Fig. 1) is the largest feature of the Phlegraean Volcanic District, which includes the islands of Procida and Ischia, as well as submarine vents in the northwestern Gulf of Naples. It lies within the Campanian Plain, an 80×30-km-wide graben, formed since the Pliocene and still affected by continuous subsidence at a rate of 1.5–2mm a^{-1} (Dvorak & Mastrolorenzo 1991). The most conspicuous geological feature of Campi Flegrei is a 12-km-wide collapse caldera outlined, on land, by a discontinuous ring of hilly morphology with inward-facing scarps enclosing the volcanic field. The caldera rim, inferred in scattered points by the stratigraphic sequence (Camaldoli Hill), ranges in elevation between about 450 m and a few tens of metres, and continues for about one-third of its depth below sea-level, forming the Bay of Pozzuoli. A few marine volcanic relics represent the submerged part of the volcanic field. The southern limits of the caldera (below the sea) are poorly known and mainly inferred by geophysical investigations. A near-vertical fault system defines the geometry of the central depression which characterizes the nearly circular caldera structure.

The intracalderic area of Campi Flegrei shows the typical features of a volcanic field characterized by different landforms (Fig. 1). It includes closely grouped volcanic hills, coalesced craters, depressions bordered by steep, eroded volcano flanks and fault scarps, crater-filling lakes, and relics of ancient marine terraces. The few major intracalderic plains of Fuorigrotta, Soccavo, Pianura, S. Vito, Quarto and La Schiana are associated with localized subsidence areas due to local movement following eruptive episodes. The coasts of Campi Flegrei can be grouped in two principal types: beaches at the termination of alluvial plains, and the steep, mostly tuffaceous, cliffs – many of which are natural sections of volcanic cones eroded by the sea or dislocated by faults (volcano-tectonic events). Littoral dunes and lagoons (Patria, Fusaro, Miseno and Lucrino lakes) created by sand-bars complete the beautiful physical setting of the territory.

Accurate geochronological analyses now supply an objective control on stratigraphic correlations and more effective constraints on the ages of the main volcano-tectonic events. The Campanian Ignimbrite (VEI = 6), which has been often thought to be associated with the early caldera depression (e.g. Rosi & Sbrana 1987) was erupted about 39 000 a BP (De Vivo *et al.* 2001), while the subsequent largest event, which generated the Neapolitan Yellow Tuff (NYT, VEI = 5), occurred *c.* 15 000 a BP (Deino
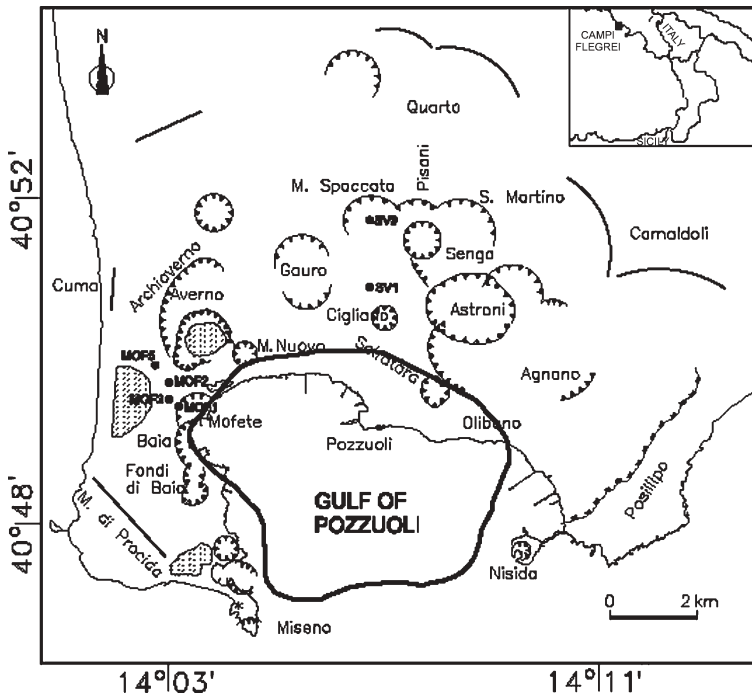
Fig. 1. Schematic map of Campi Flegrei caldera showing the main structural features (redrawn from De Natale *et al.* 1991).

et al. 2004), and caused the inner part of the caldera to collapse by several hundred metres. Indeed, the inner caldera rims, recognizable in the field and via geophysical methods, coincide with a deep dislocation in the NYT formation. Since the NYT eruption, volcanic activity have been restricted to smaller events within the caldera. To date, at least 60 eruptions have been recognized, from some tens of scattered vents (monogenetic events).

The caldera area is inhabited by about 1.5 million people. Its magmatic system is still active, as testified by the 1538 AD Monte Nuovo eruption (Di Vito *et al.* 1999); the recent bradyseismic episodes in 1969–1972 and 1982–1984 that have generated a net uplift of 3.5 m around the town of Pozzuoli; and the widespread occurrence of fumaroles and thermal springs. The combination of dense urbanization and very active short-term deformation make the volcanic risk in the area very high.

This work synthesizes the main features of recent unrest at Campi Flegrei caldera to present a coherent model for unrest episodes and to gain insights into the main issues of volcanic hazard, pre-eruptive scenarios and the impact of pyroclastic flows and falls.

Ground movements and recent episodes of unrest

Studies of slow movements at Campi Flegrei began with observations of sea-level markers on Roman coastal ruins, which were sensitive to large, secular deformation. The first – and most studied – archaeological site was the Roman market-place (Macellum) in Pozzuoli. The monument has been the object of intensive research, starting shortly after its excavation in 1750 (Breislak 1792; Forbes 1829; Niccolini 1839, 1845; Babbage 1847; Lyell 1872; Gunther 1903; Parascandola 1947). A marine mollusc, *Lithodomus lithophagus*, has bored into and left shells in three 13-m standing marble columns, recording the vertical movement of the ground with respect to sea-level. Parascandola (1947) presented the first reconstruction of historical ground movements, later modified by Dvorak & Mastrolorenzo (1991), and, in the last few years, by Morhange *et al.* (1999) (Fig. 2).

The Pozzuoli area has been characterized, since at least Roman times, by subsidence at a rate of about 1.1–1.7 cm a^{-1}, interrupted three times, once in the Middle Ages, and once about 40 years before the last eruption in 1538. After
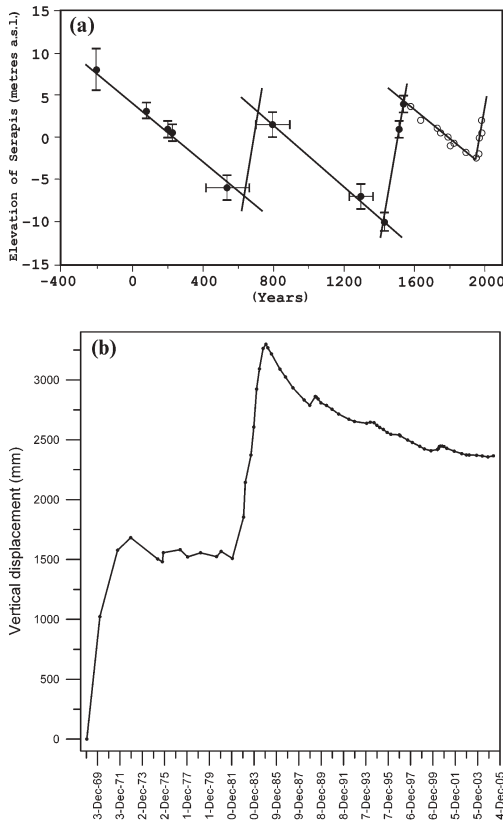
Fig. 2. (a) Schematic history of vertical movements at Macellum in Pozzuoli, known as Serapis Temple (after Bellucci *et al.*, 2006, paper 8 of this volume, pp. 141–157). Black circles represent the constraints found from radiocarbon and achaeological measurements by Morhange *et al.* (1999); white circles (post-1538) represent inferences by Dvorak & Mastrolorenzo (1991); (b) Vertical ground displacements as recorded at Pozzuoli harbour by levelling data in the period 1969–2005 (Macedonio & Tammaro 2005; Del Gaudio *et al.* 2005).

the 1538 eruption, the subsidence continued at the previous rate, until the end of 1960s, when rapid uplift started again, totalling about 1.7 m between 1969 and 1972. There followed 10 years of virtually no movement (a net subsidence of less than 30 cm) until 1982, when renewed uplift raised Pozzuoli by almost 2 m up until the end of 1984 (Fig. 2). The last two episodes of unrest (called bradyseisms, from the Greek term for 'slow earthquake') aroused concern about a possible impending eruption, causing the authorities to evacuate the town of Pozzuoli. As a result of this concern, and also beacause of the risk of damage to buildings caused by earthquakes and static deformation, Pozzuoli was evacuated.

The pattern of ground deformation during the recent bradyseismic uplift resembled an almost circular lens centred near Pozzuoli. Much recent research, expecially since the 1982–1984 unrest, has focused on the strongly confined nature of the deformation (decaying radially by more than 95% over 3 km from the maximum), on the large scale of the deformation itself (up to 1.8 m in two years, as measured at Pozzuoli harbour) and on the fact that the deformation did not culminate in an eruption. Thus, although the concentration of the deformed area indicated can be explained by the very shallow depth of the magma chamber (see, for instance, Berrino *et al.* 1984), the large amount of uplift, interpreted in terms of the classical point-source model (Mogi 1958) would acquire overpressures in the source exceeding some hundreds of MPa, depending on the source radius, large enough to be sustained by the strength of the host crust (De Natale *et al.* 1991). To accommodate more reasonable overpressures (roughly equivalent to the crust's tensile strength, about 10 MPa or less) numerous models have proposed a range of crustal rheologies, from heterogeneous elastic models (e.g. Bianchi *et al.* 1987), to visco-elastic or elasto-plastical. Regarding the source geometry, since the marked symmetry of the vertical deformation suggested an axial-symmetrical source, generally it has been interpreted either as a circular source (e.g. Berrino *et al.* 1984; Bonafede *et al.* 1986) or as an oblate spheroid (e.g. Bianchi *et al.* 1987; De Natale *et al.* 1997), eventually degenerating into a horizontal sill (e.g. Dvorak & Berrino 1991). The oblate shape was generally preferred because it maximizes the amount of vertical displacement, thus helping to minimize the extremely large overpressures required to model about 2 m of uplift. Visco-elasticity has been used both as a diffuse rheology of the whole medium (e.g. Bonafede *et al.* 1986), and as localized around the magma chamber due to very high temperatures (Dragoni & Magnanensi 1989). De Natale *et al.* (1991), however, showed that the large amount of uplift recovered during the subsequent subsidence implied that the elastic response must have continued for at least five to ten years after uplift has ceased. Any viscous effect, therefore, must have been small over the same time interval and, hence, negligible during the two years of uplift itself. De Natale & Pingue (1993) first showed that the concentration of ground deformation, whose shape remained unchanged over all the episodes of rapid uplift and subsidence, could instead be explained by localized plasticity marking the ring-faults at the caldera borders. Passive slip along these faults during inflation would produce a constant and concentrated

pattern of deformation, almost independent of the source depth (see also De Natale *et al.* 1997).

Very recently, Trasatti *et al.* (2005) presented a model in which the concentration of ground deformation is explained by the elasto-plastic behaviour of the whole crust, with a lower plastic threshold within the caldera and, consequently, a lower effective rigidity of the inner caldera structure. However, Troise *et al.* (2004) have demonstrated that the presence of ring-faults at the inner caldera borders is much more effective in producing a concentrated deformation with respect to any realistic heterogeneity of rigidity. They also pointed out that the effect of ring-faults on secular subsidence should produce a larger deformed area with respect to that involved in fast uplift and subsequent partial recovery episodes.

Another striking feature of the recent unrest at Campi Flegrei was the occurrence of a certain amount of subsidence following the uplift episodes (about 80 cm between 1985 and 2005). Oscillation of ground level between uplift and subsidence episodes, common to other similar calderas like Yellowstone (Arnet *et al.* 1997) is difficult to interpret in the light of classical models of inflation and deflation of magma chambers, when no eruption (with consequent deflation) occurs at the end of uplift episodes. In addition, the fast subsidence phase following the 1984 uplift has been punctuated by some small uplifts, of maximum amounts between 1.5 and 11 cm, with an almost constant period of five years (Gaeta *et al.* 2003). Each of the small uplifts was also accompanied by micro-earthquake swarms lasting from days to weeks (Bianco *et al.* 2004). The occurrence of earthquakes also characterized the two unrest episodes of 1969–1972 and 1982–1984, whereas no local seismicity has been observed in the absence of uplift. Weaker seismic activity was recorded during the 1969–1972 unrest, whereas a large number of earthquakes (about 15 000), with magnitudes ranging from about zero to five, was recorded during 1982–1984 (De Natale & Zollo, 1986; De Natale *et al.* 1995). A magnitude 4.2 earthquake with an epicentre in Pozzuoli occurred on 4 October, 1983.

Figure 4 synthesizes the main features characterizing the unrest in 1982–1984. Most of the seismicity occurred in the period March–April 1984, including a swarm of 550 earthquakes on 1 April. Figure 3 shows the most representative picture of seismicity during the 1982–1984 unrest in terms of earthquake density maps, computed using the Bayesian method of Presti *et al.* (2004) for the 450 best-recorded events during the period. Troise *et al.* (1997, 2003) gave a coherent model for earthquake occurrence during unrest episodes, in terms of static stress changes due
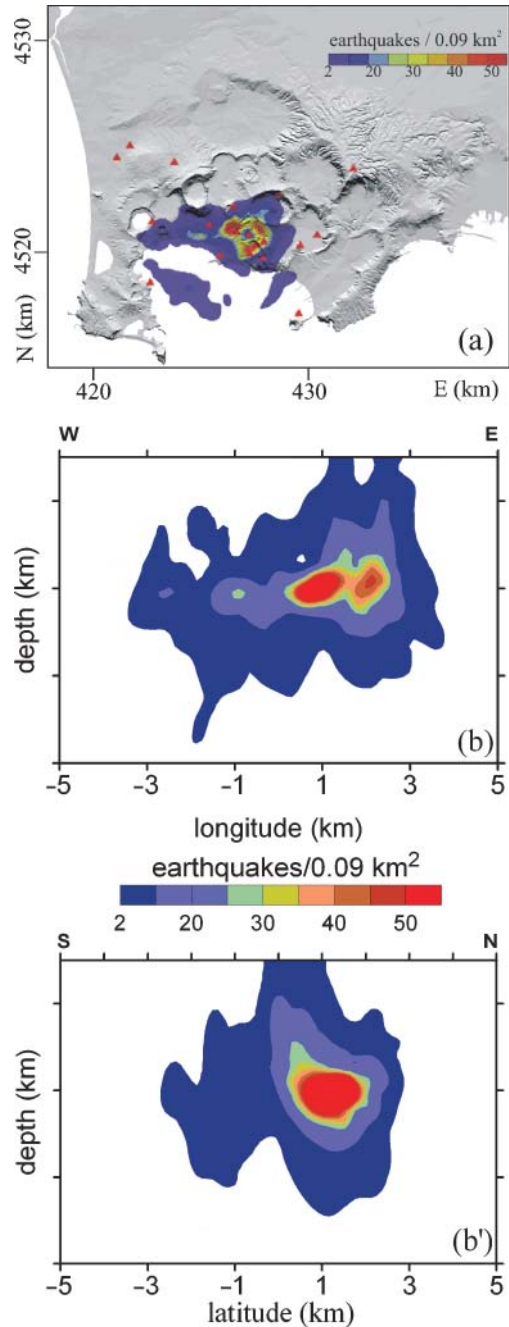

Fig. 3. (**a**) Earthquake density in the *x*–*y* plane for 370 events recorded in the Campi Flegrei area between 1973 and 1984. Events were located using a minimum number of eight arrival-time readings (after Presti *et al.* 2004); (**b**) and (**b′**) show, respectively, marginal earthquake densities along west–east and north–south sections centred at the crater axis (after Presti *et al.* 2004).
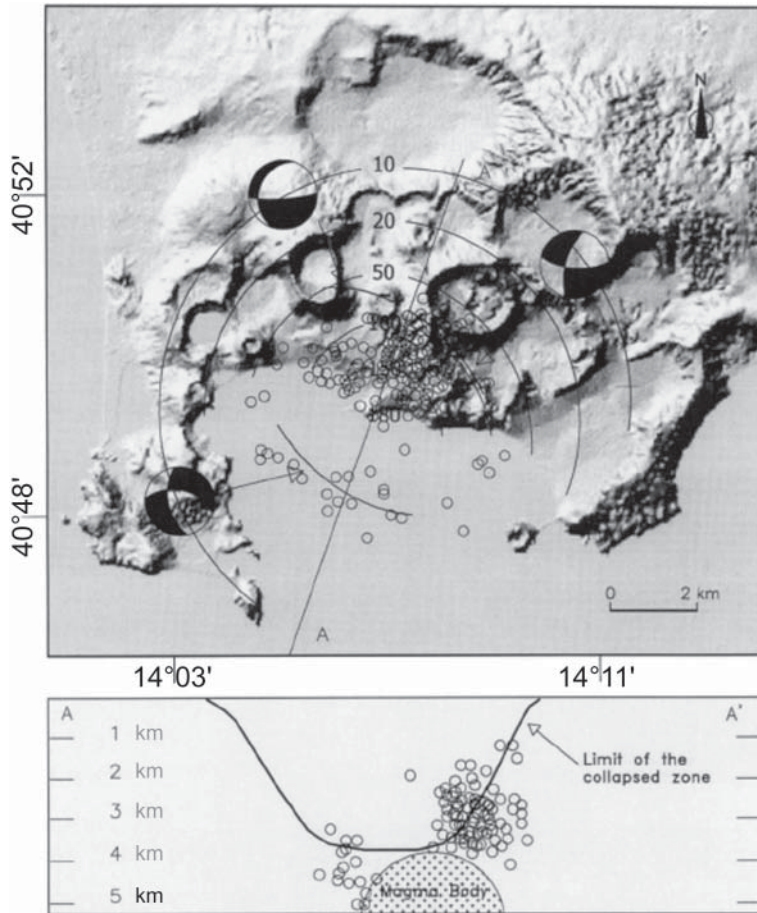
Fig. 4. Map of geophysical observations at Campi Flegrei during the 1982–1984 unrest episode. Contours of vertical displacements (in cm) and earthquake epicentres are shown; the projection of the collapsed zone as modelled from gravity anomalies is superimposed on the depth section of the hypocentres. Composite focal mechanisms computed for the different seismic zones are indicated (De Natale *et al.* 1995). Also shown is the location of the possible magma chamber, as inferred by Ferrucci *et al.* (1992) (after De Natale *et al.* 2001).

to the combined effect of the source of uplift, regional stress and the presence of ring-faults. A schematic picture of the model for earthquake occurrence during uplift episodes is shown in Figure 5b. Earthquake locations are focused in zones of maximum Coulomb fracture stress change (in red). Expected fault mechanisms for this model also agree with observations, having normal faulting dip components.

The Campi Flegrei substructure and the problem of magma-chamber location

The Campi Flegrei substructure can be constrained by several types of datasets. The first comes from deep drillings made by the Italian

Oil Agency (AGIP 1987) in the 1970s. They measured temperatures, porosity and density in several wells in the Mofete area, on the easternmost caldera rims, and at some wells at San Vito, about 2 km north of Pozzuoli (Fig. 1). In addition, information on seismic velocities has been obtained from local earthquakes recorded by the permanent and temporary seismic networks operating in the area. Most of earthquake data were collected during the 1982–1984 unrest, by the permanent monitoring network as well as a temporary digital network by the University of Wisconsin (UW) in 1984 (Aster *et al.* 1992). Data from the temporary network were used to obtain the first V_P (for P-wave velocity) and V_S (for S-wave velocity) tomographic image of
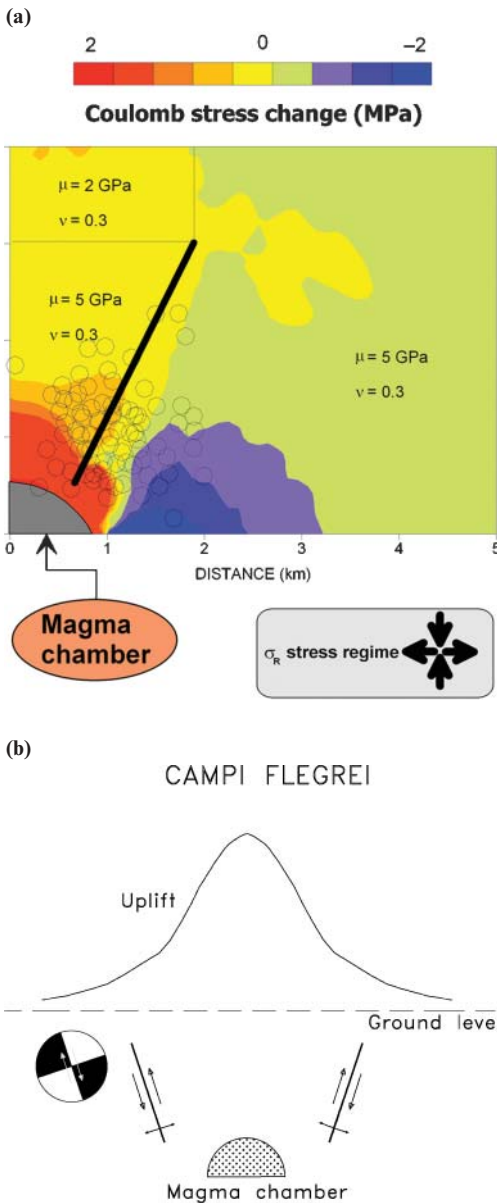
(a)

(b)

Fig. 5. (**a**) Maximum Coulomb stress changes for a spherical source (radius 1 km, depth 4.5 km and ΔP 5 MPa) embedded in elastic half-spaces and in the presence of a background extensional stress σ_R amounting to 10 MPa (after Troise *et al.* 2003); (**b**) schematic view of the movements along the ring faults produced by a spherical pressure source, compared with those generated by a normal-fault local earthquake (after De Natale *et al.* 2001). The apparent thrust fault movement along the ring faults is not seen in earthquake data, so it must be aseismic (see Troise *et al*. 1997).

Campi Flegrei (Aster & Meyer 1987). This image has recently been modified by inversion of an improved earthquake dataset, containing about 400 earthquakes recorded in the period 1983–1984 by both the permanent and the UW temporary network (Vanorio *et al.* 2005; Vinciguerra *et al.* 2006).

The third, and most informative, source of data about the shallow structure of Campi Flegrei and the surrounding area is the active seismic tomography survey made by sea shots in the Gulf of Pozzuoli (Zollo *et al.* 2003). From this dataset, profiles of seismic velocity have been obtained to depths of about 5 km, with a generally high resolution due to the high seismic frequencies involved and the design of the experiment. In addition, a conversion from P- to S-waves has been recorded during the 1987 active seismic experiments in the Gulf of Pozzuoli (Ferrucci *et al.* 1990), and during regional/teleseismic events (Ferrucci *et al.* 1992; De Natale *et al.* 2001).

Finally, useful constraints on seismic velocities can be inferred by laboratory experiments on Campi Flegrei rocks, aimed at determining seismic velocities under realistic conditions on rock samples (Zamora *et al.* 2001; Vanorio *et al.* 2005; Vinciguerra *et al.* 2006).

Further constraints are also available from gravimetric Bouguer anomalies determined by AGIP (1987) over a dense grid covering the Campi Flegrei area, and from petrological estimates of magma residence depths (Rosi & Sbrana 1987; Pappalardo *et al.* 2002).

Primary evidence for the shallow structure of Campi Flegrei is the presence of an almost collapsed area, with a radius of about 2–3 km, around Pozzuoli. This feature, which is well constrained by gravimetric Bouguer anomalies (Rosi & Sbrana, 1987) and by recent active tomographic data (Zollo *et al.* 2003), is interpreted as the inner caldera formed 15 000 a BP by the so-called Neapolitan Yellow Tuff eruption. With a maximum depth of 3 km, the collapsed basin has been filled by low-density and weakly coherent material erupted after caldera formation.

Figure 6a & b shows the maps of V_P and V_P/V_S velocities as determined from local earthquake tomography in this paper. These have been obtained by inverting 2500 P- and 1257 S-wave arrival times from 331 earthquakes detected by seismic stations (of both permanent and temporary networks) operating in the area during 1973–1984. Earthquakes were selected to have a minimum number of eight arrival-time recordings. Data were inverted using the SIMULPS13Q program (Eberhart-Philips 1998; Thurber 1993) with finite-difference 3D
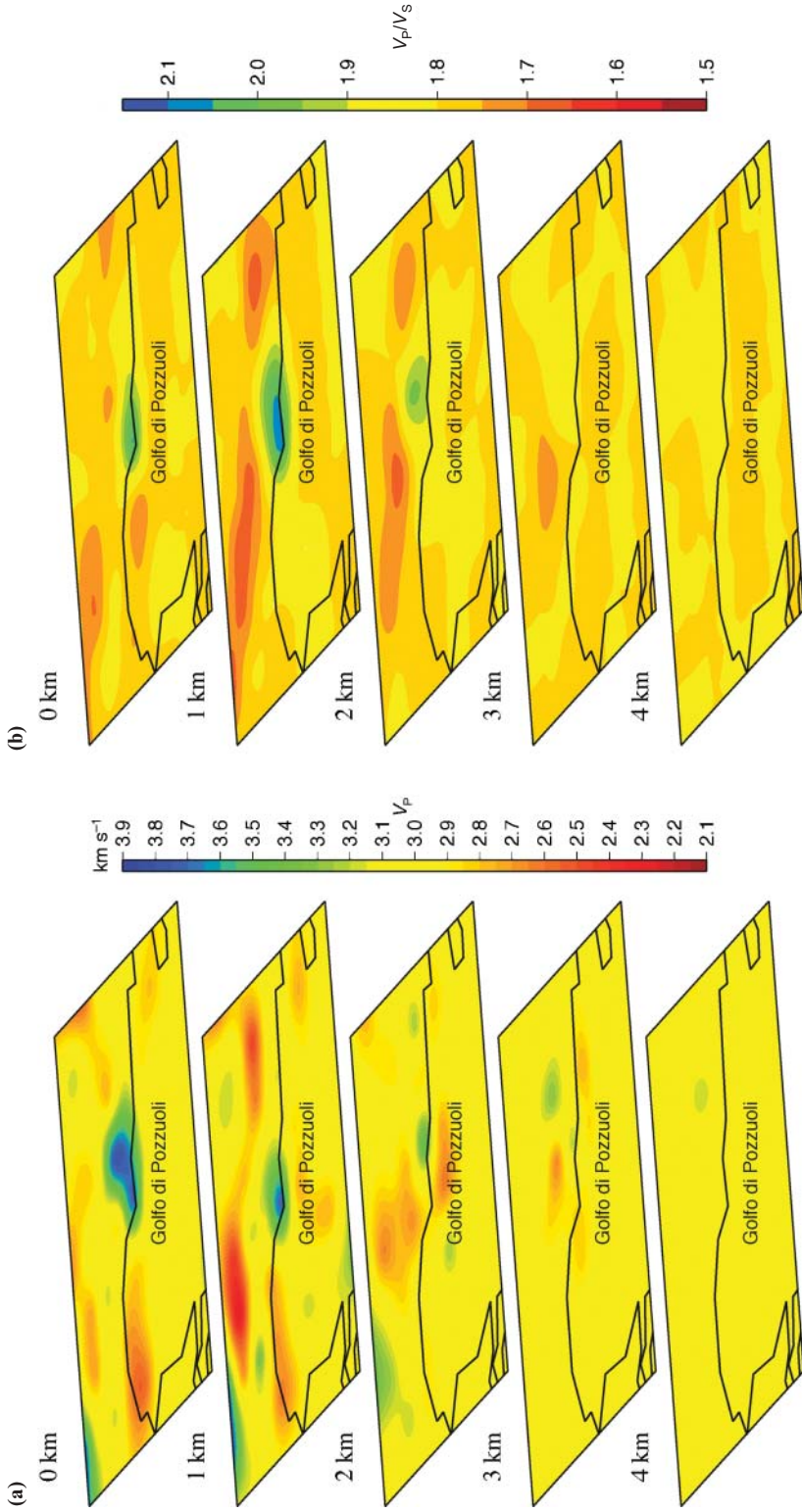
Fig. 6. (**a**) P-wave velocity distributions at Campi Flegrei at depths of 1, 2, 3 and 4 km; (**b**) V_P/V_S velocity ratio distributions at Campi Flegrei at depths of 1, 2, 3 and 4 km.

ray-tracing on a 1-km grid. Levemberg–Marquardt dampings as $\lambda_P = 7$, $\lambda_S = 12$ were chosen to optimize the trade-off between decrease of residuals and variance norm. The starting model was a half-space with $V_P = 3.0$ km s^{-1} and $V_P/V_S = 1.8$, which minimized the travel time residuals. After four inversion steps, the RMS reduction was 40%. The results indicate a zone, located around Pozzuoli between 0 and 3 km depth, with extremely high V_P/V_S (higher than 2.0), consistent with previous results (Aster & Meyer 1988; Vanorio *et al.* 2005) and average values for V_P (2.9 km s^{-1}) higher than those determined in laboratory on dry tuff samples, but agreeing well with laboratory measurements of saturated tuffs (Vinciguerra *et al.* 2006). The implication is that Pozzuoli overlies a system of shallow aquifers in an almost cylindrical volume, about 1 km in diameter, of water-saturated and fractured rock. The maximum vertical extent of the aquifers can be constrained from pressure–temperature conditions found in the Mofete wells. These indicate critical water-vapour equilibrium at a depth of about 3 km, so that water cannot be liquid below this depth threshold. It is also important to note that temperature profiles at Campi Flegrei wells give maximum temperatures of about 450 °C at 3 km, and respective average gradients of about 150 °C km^{-1}.

Local seismicity abruptly terminates at depths of 3.5–4.0 km, suggesting a sharp transition from brittle to ductile behaviour (see Hill 1992). Indeed, conversion of P- to S-waves from active shots in the Gulf of Pozzuoli and regional seismicity (Ferrucci *et al.* 1992), as well from teleseismic waves in the inner caldera (De Natale *et al.* 2001), suggest the presence of magma or, at least, hot ductile rock, at depths of 3.5–4.0 km. However, seismic tomographic surveys have not found the low-velocity anomalies expected at these depths if magma were present. Instead, they indicate zones of high velocity (6.0–6.2 km s^{-1}) between 4 and 5 km below the centre of the caldera.

In principle, if the observed P/S conversions are generated at the surface of a small magma sill, the sill could go undetected by transmission tomography, which at depths of 4–5 km has a resolution hardly better than 1 km^3. However, the problem of magma detection by tomographic methods, mainly at calderas, is much more general. Calderas, in fact, are volcanic areas formed by huge quantities of erupted magma, and hence imply the existence of large magma chambers, with typical volumes in the order of 100–1000 km^3 and more. Generally, although the use of seismic tomography is now rather widespread worldwide, almost no evidence is found for large, shallow magma chambers at calderas,

compatible with petrologically inferred volumes. On the contrary, high velocities are more often found at depths where shallow magma chambers would be expected (Zollo *et al.* 1996; Chiarabba *et al.* 1997; Chiarabba *et al.* 2000; De Natale *et al.* 2004). At Long Valley caldera, for instance, shallow bodies (marked by low V_P) have been found (Weiland *et al.* 1995), but much smaller than the huge volumes of original magma chamber as required by petrological inferences. Such worldwide negative evidence for molten residual magma could be interpreted as being due to the fact that residual magma after large eruptions is generally strongly crystallized (i.e. a mush). An effective mechanism for sudden crystallization well before the long times required by cooling of considerable volumes of molten rock, is rapid degassing during eruptions (De Natale *et al.* 2004). In this hypothesis, subsequent large eruptions could be driven by inflow of new volatiles (mainly water) in the mushy magma chambers, remelting the previous magma, and/or by new amounts of molten magma.

Zollo *et al.* (2003) interpreted the high-velocity layers below 4 km as limestones and inferred that any major magma reservoir should lie at greater depths. An alternative interpretation is that the high-velocity layers represent solidified magma. According to Schon (2004), seismic velocities, in the order of 6.0–6.2 km s^{-1} at a depth of 4 km are consistent both with solidified lavas at 4–6 km and water-saturated limestones, but are too high for dry limestone. Given the maximum depth of 3 km for water to exist (from Mofete data), the interpretation could be that the high-velocity zone reflects levels of solidified magma. Moreover, such an interpretation naturally accounts for the presence of high velocities in the depth range where residual magma is expected after caldera formation (Burov & Guillou-Frottier 1999). The abrupt termination of seismicity below 4 km could also be explained in terms of brittle–ductile transition at this depth, coinciding with an increase in temperature above 500–600 °C (Waite & Smith 2002). Indeed, simple extrapolation of the temperatures and gradients measured at the deepest Mofete well indicates minimum values of 600 °C at depths of 4 km (AGIP 1987; Gaeta *et al.* 1998). A similar conclusion was reached by De Lorenzo *et al.* (2001), who analysed the anelastic attenuation of seismic waves to constrain a thermal model for the Campi Flegrei substructure.

In conclusion, provided that the subsurface conditions measured at the Mofete wells can be considered representative of all the inner-caldera rocks, the shallowest magma chamber is most likely to be located at depths greater than 4–6 km. Most of the magma is expected

to be degassed and, hence, mostly crystallized, although small batches of molten magma may exist and pass undetected by transmission tomography, especially if stored in small sills. The strong P to S conversions observed at depths of about 3.5–4 km could be produced by such a sill or, alternatively, by a lens of magmatic fluids located just above the magma chamber, which is typical of any volcanic geothermal systems (Fournier 1999). Petrological data indicate preferred depths for magma residence of 5–8 km and 10–15 km (Pappalardo *et al.* 1999; Pappalardo *et al.* 2002). Such depths are very similar to those inferred for magma storage below Vesuvius (Pappalardo *et al.* 2004; De Natale *et al.* 2006). The resulting tentative reconstruction of the Campi Flegrei substructure is shown in Figure 7.

A mixed magmatic fluid-dynamic model for unrest episodes at Campi Flegrei and similar calderas

The peculiar time behaviour of ground deformation at Campi Flegrei (Fig. 2) with fast uplift and subsequent subsidence without eruptions, calls
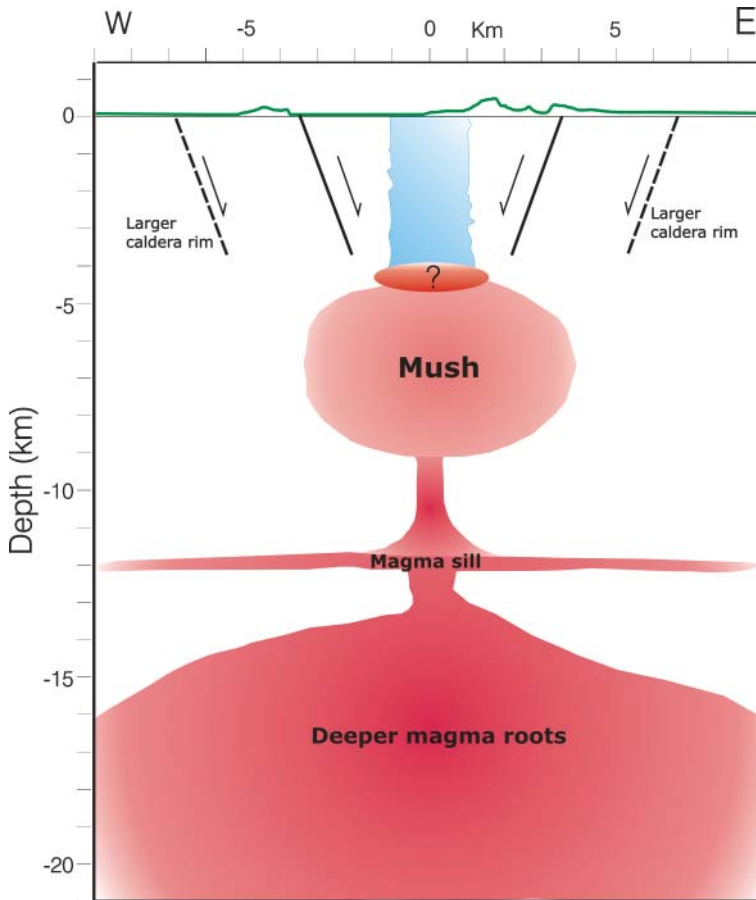

Fig. 7. Tentative schematic reconstruction of the Campi Flegrei substructure. The central aquifer is schematically shown in blue, as inferred from V_P/V_S anomalies. A possible shallow, small magma chamber could be located at *c.* 4–4.5 km depth. The schematic picture of the hypothesized magma chambers below 4–5 km is mainly based on petrological data (e.g. Mastrolorenzo *et al.* 2004). The large residual magma chamber responsible for the caldera-forming eruptions could be now almost totally crystallized (mush), giving the high velocities inferred by recent active tomography (Zollo *et al.* 2003). Below 10 km, petrological data infer another magma source, which could be in relation to the large sill under the Campanian volcanoes, as inferred by Judenherc & Zollo (2004). Deeper magma roots are based on regional tomographic studies by De Gori *et al.* (2001). The inner-caldera collapse, surrounded by buried ring-faults, is shown by continuous lines. The apparent limits of a larger caldera are shown by broken lines.

for a mechanism of inflow and outflow of fluid from the system. Several papers have interpreted such evidence in terms of the involvement of the shallow geothermal system in the unrest episodes (Bonafede 1991; De Natale *et al.* 1991; Gaeta *et al.* 1998; Troise *et al.* 2001; Chiodini *et al.* 2003).

To test this interpretation we here consider the ground deformation and microgravity changes measured at this area (Battaglia *et al.* 2006). Since ground deformation constrains the volume changes at depth and microgravity constrains the mass change, the two datasets together can constrain the density of the fluid involved. In our analyses we firstly consider a homogeneous, non-fractured medium; further, we show the modifications introduced by considering the presence of ring-faults marking the caldera borders.

Joint inversion of deformation and gravity changes

The temporal gravity change Δg determined by differencing repeated gravity measurements is controlled by the sum of four elements: (1) the free-air effect, proportional to the uplift h; (2) the water-table effect, Δg_w; proportional to the effective porosity φ_e and water-table change δz; (3) the deformation effect Δg_D; and (4) the residual gravity Δg_R, which depends on the mass change accompanying the deformation (Eggers 1987; Battaglia *et al.* 2003).

We use the theoretical value of the free-air gradient rather than the local observed value (Berrino *et al.* 1984) to compute the free-air gravity correction, because the theoretical value better represents the change of gravity due to uplift at the caldera scale. Measured free-air gradients are strongly influenced by terrain and local effects that will cancel out in differential gravity surveys (Lafeher 1991).

Since there are no direct measurements of water-table changes that cover the time span of our study, we computed the water-table recharge $\varphi_e \delta z$ using a cumulative rainfall departure (CRD) method (Xu & van Tonder 2001). In coastal aquifers, taking into account urban development, the recharge is about 30 to 40% of the CRD (Appleyard 1995). Because of the limited recharge, the water-table effect is negligible during the time span of our investigation.

The deformation effect Δg_D is the result of subsurface mass redistribution due to a dilatational source (Walsh & Rice 1979). This effect is exactly zero if the source has a spherical symmetry (Walsh & Rice 1979), but can strongly bias the density estimate for a horizontal penny-shaped crack (Table 1).

Our data include levelling, EDM and gravity measurements collected by the Osservatorio Vesuviano (Fig. 8). The analysed periods have been chosen in order to include horizontal deformation data in time intervals comparable with the other data, given that EDM data were only occasionally collected in the considered period. First-order optical levelling data, referenced to the first Benchmark in Naples, are available for the whole period 1980–1995. Distance changes in an EDM network covering the caldera were determined for 13 baselines between 1980 and 1983 (during inflation; Dvorak & Berrino 1991), and 21 baselines between 1991 and 1995 (during deflation; Berrino 1995). Our computations in this paper will assume a homogeneous, elastic,

Table 1. *Summary of the joint inversion of geodetic and gravity data**

Model	χ_v^2	Z	ΔV	$\Delta P/\mu$	ρ	ρ^*	R	A
			1980–1983 (During inflation)					
Poi	17	3.0	33	–	3.0	3.0	–	–
Sph a	16	2.8	28	0.009	3.1	3.1	1	1
Sph b	16	2.8	28	0.07	3.2	3.2	0.5	1
Pen	2	2.6	21	6×10^{-4}	0.6	4.6	2.4	–
			1990–1994 (During deflation)					
Pen	1.5	3.6	−5	$−6 \times 10^{-4}$	−1.1	2.3	1.6	–
Poi	1.5	3.0	−6	–	1.4	1.4	–	–
Sph a	1.3	2.1	−6	−0.008	1.0	1.0	1.0	0.45
Sph b	1.3	2.0	−5	−0.05	1.0	1.0	0.5	0.5

*χ_v^2: chi-square per degree of freedom; Z: depth (km); ΔV: volume change (10^{-3} km^3); ΔP: pressure change; μ: shear modulus; ρ: density – taking into account the deformation effect (g cm^{-3}); ρ^*: density – assuming the deformation effect is negligible (g cm^{-3}); R: radius (km); A: aspect ratio. Pen: penny-shaped crack; Poi: point source; Sph: prolate spheroid.
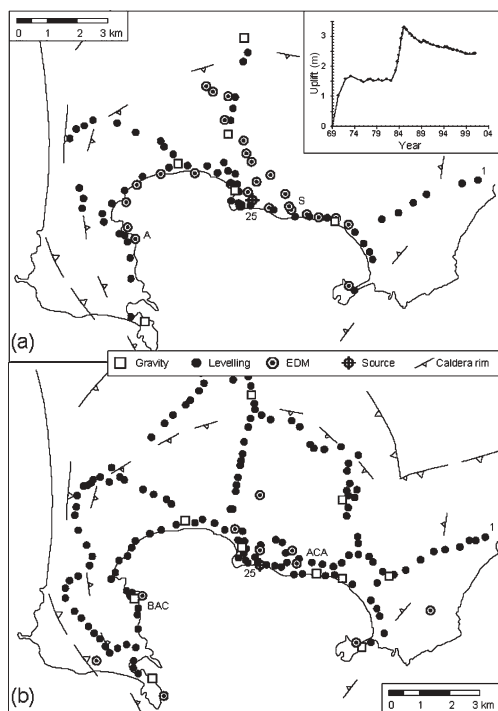
Fig. 8. Sketch map of the levelling lines, EDM, gravity benchmarks and source location at different periods of time, as analysed in this work. (**a**) Between 1980 and 1983 (during inflation); (**b**) between 1990 and 1995 (during deflation).

non-faulted medium; later in the paper we will discuss the modifications introduced in the model, considering the presence of ring-faults firstly shown by De Natale & Pingue (1993) and De Natale *et al.* (1997). The possible effect of non-elastic (i.e. visco-elastic) rheology is not considered here but, as demonstrated by De Natale *et al.* (1991), it should not be significant. Six gravity stations are available for our analysis between 1981 and 1983, increasing to 10 stations between 1991 and 1995 (Berrino 1994; Gottsmann *et al.* 2003).

The data have been inverted using a weighted least-squares algorithm with an exhaustive grid search. The covariance matrix of the solution, besides the measurement error, includes an error of 2 mm, taking into account the instability of the measuring stations. The best-fit model is determined using a reduced chi-square test, and 95% confidence limits are computed by a bootstrap percentile method (Efron & Tibshirani 1986). We test three source geometries: a spherical source (McTigue 1987), a vertical prolate spheroid (Clark *et al.* 1986; Yang *et al.* 1988), and

a horizontal penny-shaped source (Fialko *et al.* 2001), all in an elastic, homogeneous, isotropic half-space.

Our results are synthesized in Table 1 and Figure 9. They show that the deformation and gravity data during inflation are best described by changes in a horizontal penny-shaped crack, between 3.2 and 5.4 km across and 2.5–3.5 km below Pozzuoli. This implies that the increase in volume is between 0.021 and 0.027 km^3 for a fluid with density between 142 and 1115 kg m^{-3} (Fig. 9a). In contrast, the best-fit source for the deflation period is a vertical prolate spheroid 1.9 to 2.2 km deep, with aspect ratio (the ratio between the semi-minor and the semi-major axes) from 0.39 to 0.54; volume decrease from 0.005 to 0.006 km^3; and a density between 902 and 1015 kg m^{-3} (Fig. 9b) The inversion is insensitive to the magnitude of the spheroid semi-major axis (Table 1).

The best-fit results from joint inversion of ground deformations and gravity changes suggest that the bradyseismic movements since 1982 have been controlled by pressure changes in two water-rich horizons. The deeper horizon is a sill-like reservoir above the magma chamber, at 3.5–4 km depth. The upper horizon, at 1.8–2.4 km depth, has the form of a prolate spheroid and so has the depth and shape consistent with the shallow geothermal systems from seismic tomography studies and geothermal exploration wells (De Natale *et al.* 2001). The large difference in the source shape between the uplift (a penny-shaped crack) and subsidence (a vertical prolates spheroid) phases is unambiguously constrained by the large differences in the ratios between horizontal (u_r) and vertical (u_z) deformations. This ratio is larger for vertically elongated sources, whereas it is minimal for horizontally elongated ones. In terms of maximum displacements (in this work we use line elongations as horizontal data), a Mogi (1958) model has a ratio of about 0.35, which is also similar for spherical sources in general. The following is an example from our data: the ratio is 0.5 along the S–C EDM baseline ($u_r = 0.4$ m and $u_z = 0.8$ m at benchmark 25) between 1980 and 1983 (uplift); the ratio is 0.85 along the ACA–BAC EDM baseline ($u_r = 0.128$ m and $u_z = 0.151$ m at benchmark 25) between 1990 and 1995 (subsidence).

To account for the observed patterns of ground deformation and gravity change, we propose that the 1982–1984 inflation was driven by hypersaline brine and gas, which, escaping from crystallizing magma, accumulates in a horizontal lens above the magma chamber. A self-sealed zone of impermeable material separates this lens from the shallow aquifers. When a major breach of the self-sealed zone occurs (some time between
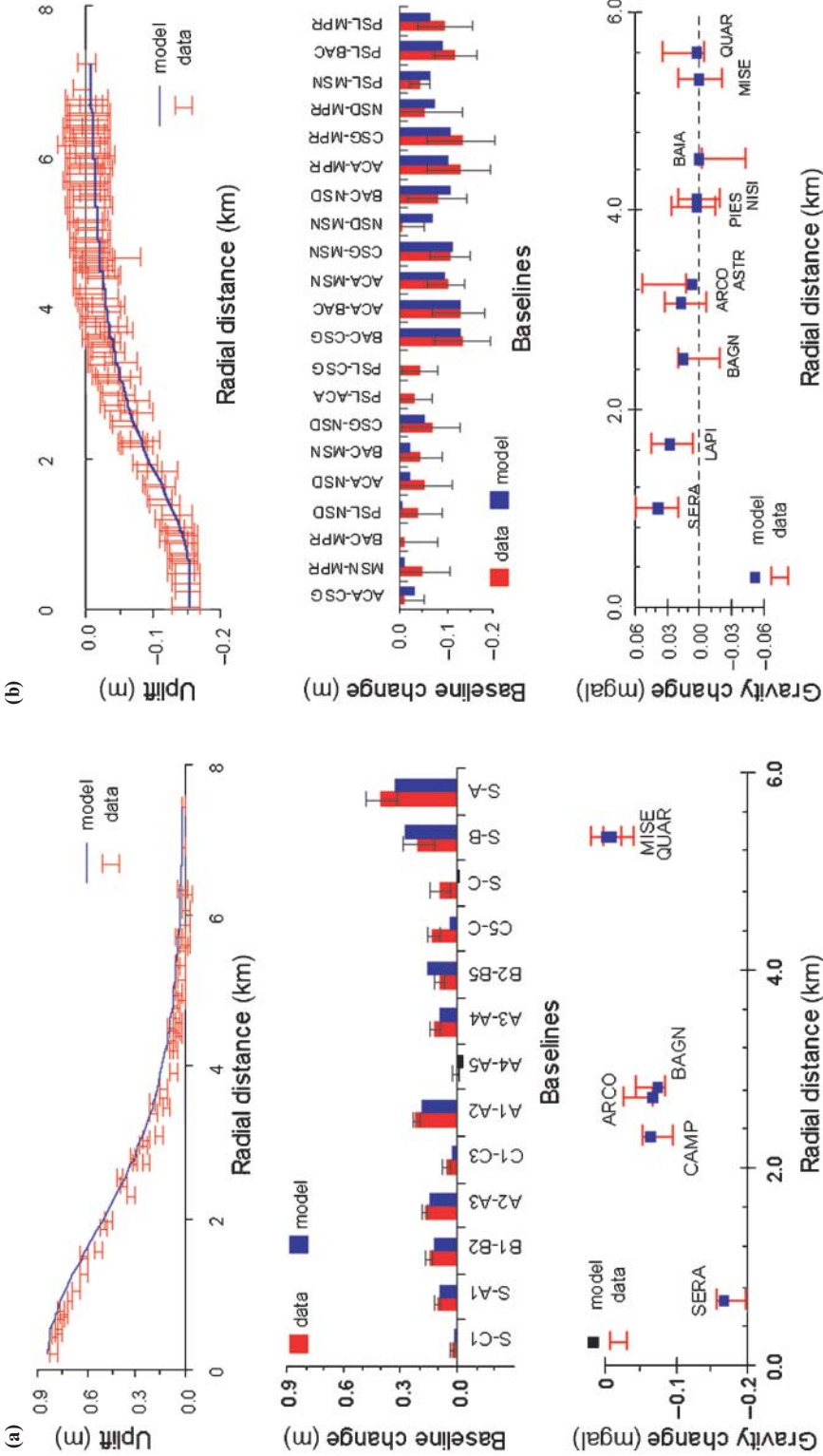
Fig. 9. (a) Fit between the data and the horizontal penny-shaped crack model (see Table 1 for source parameters). Levelling: January 1981 to September 1983; EDM: September 1980 to September 1983; gravity changes Δg from February 1981 to September 1983. No major deformation episode was detected between September 1980 and January 1981. The average deformation rate between 1974 and 1981 was 0.001 ± 0.002 m a^{-1} (after Battaglia *et al.* 2006). (b) Fit between the data and the vertical prolate spheroid model (see Table 1 for source parameters). Levelling, June 1990 to January 1994; EDM: November 1991 to June 1995; gravity changes Δg from June 1991 to January 1995. The subsidence rate was 0.015 ± 0.006 m a^{-1} in 1990–1994, and 0.012 ± 0.006 m a^{-1} in 1991–1995 (after Battaglia *et al.* 2006).

1983 and 1985), brine and gases migrate to the lower pressure and colder aquifers in the brittle crust (Fournier 1999). The consequent fluid accumulation in the shallower aquifer, would amplify the deformation, because the amount of uplift increases as the depth of the pressure source decreases. Subsidence starts when the resulting increase in fluid pressure and temperature within the brittle aquifer leads to faulting and fracturing, which increases the permeability and allows an increase in the rate of discharge of hydrothermal fluids. Lateral migration of fluids outside the caldera can be an efficient discharge mechanism (De Natale *et al.* 2001).

Although this model can explain bradyseismic movements in terms of pressure changes and fluid migration in aquifers, it does not directly address the process that initially disturbed conditions in the lower aquifer. One possibility is a sudden increased output from the magma chamber, perhaps as a response to new magma injected from below. A magmatic trigger for the unrest cannot be completely excluded by the previous results obtained for a homogeneous crust. Indeed, the effect of ring-faults at calderas makes surface deformations almost insensitive to the source depth, within a certain depth interval. Given that the source depth is only constrained by surface displacement data, the use of a homogeneous crust may underestimate its actual value. Thus, a pressure source with a centre at 5 km depth could optimally fit displacement data, with almost the same overpressure, provided that the effect of ring-faults is considered (De Natale *et al.* 1997, 2001; Beauducel *et al.* 2004). If the depth of the sill source is increased to 5 km, the surface gravity change caused by the intruded mass will be decreased, because this depends on $1/R^2$ (where R is the depth). Hence, a higher density of intruding fluid would be required to produce the observed gravity change. As a first approximation (neglecting the change of deformation effect Δg_D with depth), the decrease in gravity change from a depth of 3 to 5 km is in the order of 9/25, so that fluid density must be multiplied by 25/9 to reproduce the observed changes. The resulting values would, therefore, lie in the range 394–3090 kg m^{-3}, i.e. embracing the densities for both water and magma.

It is important to stress that the presence of ring-faults would have almost no effect on the depth of the deflation source, because the observed high ratio between horizontal and vertical deformation can only be reproduced by a very shallow, vertically elongated source. In fact, the effect of ring-faults does not significantly affect the maximum horizontal/vertical displacement ratio (Fig. 10), high values for which can only be justified by a source depth and shape similar to that found in a homogeneous crust. To prove this in a clear way, we have computed, and showed in Figure 10, the maximum horizontal/vertical displacement ratio as a function of source depth and ellipticity (ratio between the maximum and minimum axes of a prolate spheroid, taken as 0.5, 0 and 2.0 respectively) in an axial-symmetrical homogeneous half-space with ring-faults. The resulting source depth and shape have values very similar to those found in a continuous crust.

The subsidence phase following fast uplift at Campi Flegrei is thus most likely to be caused by a shallow source, elongated vertically. The fast uplift itself, however, may be considered to have been caused by changes in a deeper magma body or a water/gas-filled reservoir. The preferred model involves a first phase of uplift produced by a sill-like source filled by magmatic fluids or magma itself; magmatic fluids then migrate into the shallow aquifers, amplifying progressively the ground deformation which depends on $1/R^2$ ($R=$depth). After reaching the maximum pressurization of the whole aquifer, water tends to flow out of the caldera, causing the subsidence phase immediately following the uplift.
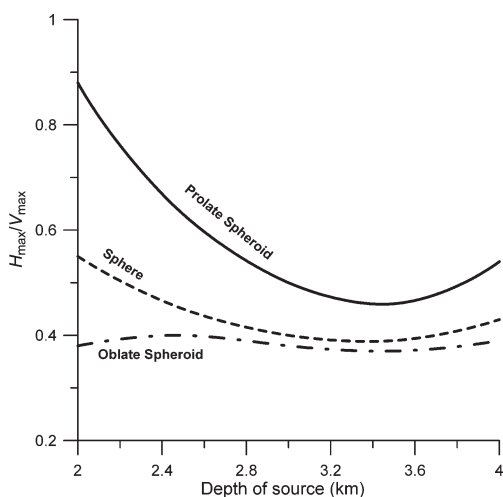

Fig. 10. Maximum horizontal/vertical ratio *v.* source depth in the case of three sources with different geometries (prolate ellipsoid, sphere, oblate ellipsoid) embedded in an elastic half-space with ring-faults located to simulate Campi Flegrei Caldera.

Implications of the model for possible pre-eruptive processes

The model obtained in our study has fundamental implications for forecasting eruptions at Campi Flegrei and similar calderas. Part of the uplift (in our case the deformation between 1982 and 1984) is amplified by perturbations of the geothermal system. Hence, if the triggering process is magma intrusion, it must take place at the beginning of the crisis; subsequent subsidence, in turn, represents lateral outflow of water from a shallow aquifer. An immediate consequence of this model is that the maximum uplift is not directly associated with a maximum in magma overpressure, but instead to a delayed response of the geothermal aquifer. The maximum hazard for an eruption is therefore at the beginning of unrest, in correspondence with the magmatic input. In addition, if the initial input corresponds to the injection of new magma, the cumulative effect of several unrests would be to accumulate magma overpressure in the chamber. The eruption could then occur when, after a certain number of consecutive unrests episodes, cumulative magma pressure overcomes the threshold of rock strength (Fig. 11). Such a model is also consistent with conditions observed in 1994 at Rabaul Caldera, New Guinea (Nairn *et al.* 1995) where eruption from two vents began about twelve hours after the start of weak precursory
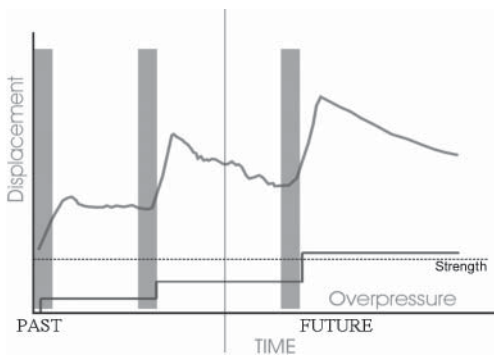

Fig. 11. Schematic view of vertical displacements as a function of magmatic source overpressure. In this sketch, for a fluid-dynamic model with magma overpressure as the initial input, most of the ground deformation is caused by a delayed response from aquifers. In this case, the highest eruptive hazard should be at the beginning of the unrest (shaded intervals), not during the phase with the largest uplift. Eruption occurs when the rock strength (dashed line) is overcome by the cumulative overpressure built by several consecutive periods of unrest.

signals (a seismic swarm of low-frequency earthquakes). Significantly, the eruption occurred ten years after the end of a more than a decade-long episode of geological unrest involving more than two metres of uplift and intense seismicity, which may have brought the crust to a state of instability. The model in Figure 11 may thus describe a general pattern of behaviour for calderas. If so, eruption forecasts should rely mainly on the detection of a new magmatic phase, which presumably has much less effect on observable data with respect to the spectacular ground deformation and seismicity which characterize a mature unrest. The magmatic input, representing a deeper source, should have a minor effect on surface deformation. Also important, at least in Campi Flegrei, is that the seismicity started about two months after ground deformation, so that seismicity cannot be relied upon to reveal the very first stages of unrest. Obtaining data that are more sensitive to an initial magma input from depth may thus require high-sensitivity borehole dilatometry or microgravimetry.

The key results, therefore, are that, against the background of significant geophysical anomalies observed during unrest that does not include eruptions, true eruption precursors can be very small and difficult to detect, so requiring extreme care in data acquisition and analysis. Such constraints provide useful insights into improving the monitoring network at Campi Flegrei, even if it is already one of the most well-monitored volcanic areas in the world. A very important step in future research should then be the physical characterization of the most probable true precursors of eruptions, which could involve either very small initial deformation and/or the formation of an eruption pathway by progressive earthquake fracturing (Kilburn & Sammonds 2005).

Probabilistic estimation of eruptive products hazard

The key issue for a highly explosive volcanic area like Campi Flegrei, an extremely populated region, is the accurate estimation of hazards from eruptions, and their impact on urbanz areas. In particular, it is important to estimate the probability of occurrence, at each point of the area, of the two main eruption products which constitute the highest risk: pyroclastic currents and the fallout products (ash, pumice, etc.). Despite the progress made in the last decade on the rigorous modelling of pyroclastic flows generated by explosive eruptions (i.e. Neri *et al.* 2003) these
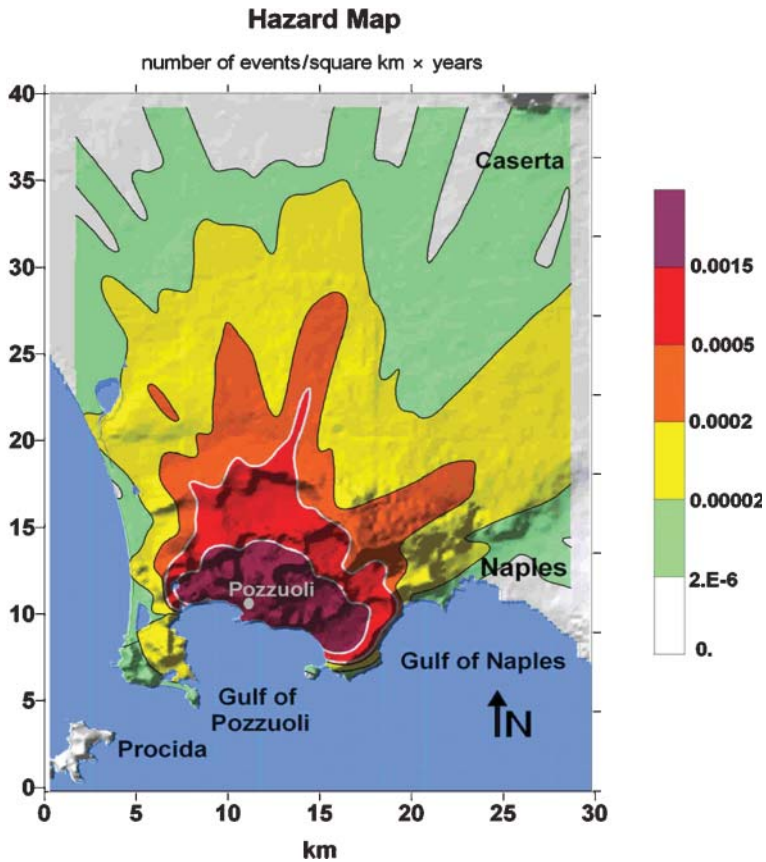
Hazard Map

number of events/square km × years

Fig. 12. Probabilistic hazard map from pyroclastic currents in the Campi Flegrei area, computed from the distribution of eruptions in the last 5000 years. The value gives the yearly probability that each small area of a square kilometre will be hit by a pyroclastic current (after Rossano *et al.* 2004).

methods are also too cumbersome even for powerful parallel computers to make a probabilistic analysis, which requires a huge number of simulations to reproduce and randomize all of the likely possible kinds of eruptions. Moreover, finite difference fluid-dynamic models require a large number of parameters to be specified, which are mostly unknown, and cannot handle a large number of grain sizes in the flow, as it is observed in the field (continuous granulometry). This is the reason why, for hazard evaluation, models which approximate the flows in terms of simple rheological models have been widely used in the last two decades (Sheridan 1979; McEwen & Malin 1989). Rheological models, which use the most general Bingham rheology, also include a particular example of the Newtonian model, allow in practice to model the heavier part of the flow, which flows on the ground under the combined effect of the initial acceleration and

the topography. Such an approximation is good enough if the flow is gravity-driven, and, as shown in many analyses (see, for instance, Neri *et al.* 2003) holds in particular for flows with grain sizes higher than about 10 μm, which is a very low threshold for most of granulometries effectively observed in pyroclastic flows at Campi Flegrei. In addition to pyroclastic currents, another important source of hazards is represented by light material in plinian columns which falls on the ground, and whose accumulation can cause roofs to collapse. Several theoretical methodologies exist, almost all based on the first models of Suzuki (1983) and Connor *et al.* (2001). Although plinian columns are not the most common explosive type in this area, this kind of phenomenon has occurred in the past and its hazard potential can be quantified. The basic method used by volcanic geologists to map hazard potential is based on the direct mapping

of past eruptive products (Connor *et al.* 2001). Obviously, such a method is largely unsatisfactory because the past eruptive history, provided that it can be well reconstructed, gives a very uneven and inadequate sample of the whole spectrum of possible eruptions, making meaningless any statistical assessment of hazards that has been constructed on such a basis. Mainly at a large volcanic field as large as Campi Flegrei, in fact, the probabilistic reconstruction of the hazard potential requires us to consider the fact that any type eruption that in the past has occurred once at a certain site, in principle can occur at any place in the caldera. Recently, Rossano *et al.* (2004) presented a rigorous volcanological–statistical procedure to construction hazard maps from records of pyroclastic currents. The resulting map for Campi Flegrei, giving the yearly probability of any site being hit by a pyroclastic current, is shown in Figure 12.

In addition, the basic methodology can be easily generalized to create hazard maps for any type of eruptive product. In the following section, we show a reconstruction of fallout hazard in the area based on a similar probabilistic method.

Pyroclastic fallout

The transport of tephra in the atmosphere, due to the processes of convection, diffusion and settling, may be described by the following well-known convection–diffusion–migration equation (Friedlander 1977), written here in conservation form:

$$
\frac{\partial \chi}{\partial t} + \frac{\partial u\chi}{\partial x} + \frac{\partial v\chi}{\partial y} + \frac{\partial w\chi}{\partial z}
$$
$$
= \frac{\partial}{\partial x}\left(K_x \frac{\partial \chi}{\partial x}\right) + \frac{\partial}{\partial y}\left(K_y \frac{\partial \chi}{\partial y}\right) + \frac{\partial}{\partial z}\left(K_z \frac{\partial \chi}{\partial z}\right) \quad (1)
$$
$$
- \frac{\partial V_{ts}\chi}{\partial x}
$$

where χ is the concentration of tephra (kg m^{-3}), $\mathbf{v} \equiv (u,v,w)$ is the wind velocity vector, K_x, K_y, K_z are diffusion coefficients, and V_{ts} is the terminal settling velocity. Where a low volume concentration of tephra is hypothesized, $\mathbf{v}$, K_i and V_{ts} depend only on (x,y,z,t) but not on χ, so the equation is linear. Given an expression for such coefficients and suitable boundary and initial conditions, eq. (1) may be solved numerically to give $\chi = \chi(x,y,z,t)$. The mass distribution of tephra after all the particles have settled may then be calculated by the integration of vertical fluxes at the surface, at a time sufficiently longer than the settling time of the smallest particles that we

are interested in. However, such an approach is computationally expensive: in order to calculate the 2D distribution of tephra on the ground for $t_F > t_s$, we have to compute a 3D field for all times $t < t_F$. According to Suzuki (1983), we can neglect vertical diffusion and convection in the atmosphere with respect to horizontal diffusion and convection because the former has a much smaller effect than the latter above the atmospheric boundary layer. We have:

$$
\frac{\partial \chi}{\partial t} + \frac{\partial u\chi}{\partial x} + \frac{\partial v\chi}{\partial y} = \frac{\partial}{\partial x}\left(K_x \frac{\partial \chi}{\partial x}\right) + \frac{\partial}{\partial y}\left(K_y \frac{\partial \chi}{\partial y}\right) (2)
$$

Now χ has the meaning of mass of accumulated tephra for unit surface (kg m^{-2}). The settling term is implicitly taken into account by considering the solution of eq. (2) at the time corresponding to the fall time of the particles. Diffusion is assumed to be isotropic ($K_x = K_y = K$), with wind velocity depending only on z, and the diffusion coefficient is assumed to be constant in space and time.

The method to solve equation (2), and to obtain a simulated 2D distribution on the ground of tephra thickness as a function of a set of eruption parameters, is described in Mastrolorenzo *et al.* (2006).

Hazard maps are generated by simulating many eruptions, grouped according to VEI (volcanic eruption index) from 0 to 5, each with a distinctive probability according to the volcanic history of Campi Flegrei.

The different values of eruption parameters for each VEI are assumed with distinctive probabilities according to the inferred features of past eruptions, on the basis of the study of their deposits. Wind velocity and direction statistics are taken from meteorological archives (see Mastrolorenzo *et al.* 2006, this volume).

For each eruption of probability p, the height h of deposited tephra at each point (x_m, y_m) of the map is calculated from the grid (x_i, y_i) of the possible eruptive vents. For each (x_m, y_m), we assign h to one of m bins I_i covering all possible values, and add the probability p to the corresponding bin. Repeating this process for all eruptions, we obtain a probability histogram of the height of deposited tephra for each point (x_m, y_m). This gives the complete statistical description of the random variable h, so now we can compute the probability of h being higher than a given threshold, the mean value of h and so on, deriving the corresponding isomaps. The hazard map for tephra fall so computed is shown in Figure 13, which gives the yearly probability of a fall-out loading larger than 200 kg m^{-2} ($h > 0.2$ m).
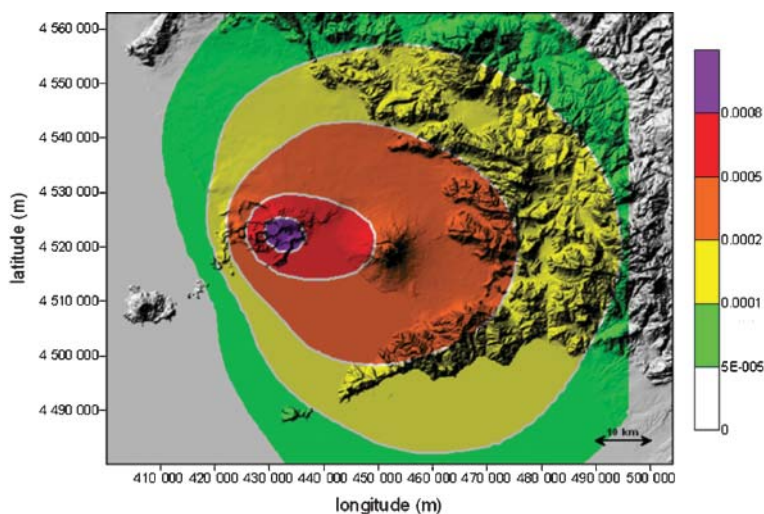
Fig. 13. Probabilistic hazard map derived from the tephra fallout pattern in the Campi Flegrei area (after Mastrolorenzo *et al.* in prep; see also Mastrolorenzo *et al.* 2006, this volume). The map gives the yearly probability that each 1 km^2 area will experience a pyroclastic fallout loading of more than 200 kg m^{-2}.

Conclusions

Campi Flegrei has been one of the world's most active calderas in the last 40 years, generating unrest phenomena not followed by eruptions, characterized by huge ground deformation and seismicity. Data from Campi Flegrei shed light on several peculiar features of caldera dynamics, and help to constrain many details of the substructure. In particular, large amounts of uplift (up to 3.5 m in 15 years) and uplift rates (up to 1 m a^{-1}), sometimes followed by partial subsidence, are explained in terms of an initial magma input followed by pressurization of the geothermal system, which then progressively deflates by water outflow. The water deflation phase, associated with the subsidence following large uplift episodes, is strongly constrained by gravity and ground deformation data, which uniquely indicate that the subsidence source is a shallow (about 2 km), vertically elongated type, with fluid characterized by densities in the range 500–1 000 kg m^{-3}.

The mixed magmatic–geothermal model for unrest episodes takes into account all the possible effects linked to the structural effects of calderas on ground deformation. Such effects, firstly evidenced by modern research on this caldera, mainly involve the passive slip of collapse ring-faults in response to the overpressure in magma chambers and aquifers. Local seismicity is shown to be also linked to the Coulomb stress changes produced by overpressure sources and ring-fault

passive slip, in a background normal-faulting regional stress regime.

Studies of the Campi Flegrei substructure, involving gravimetric data, earthquake locations, active and passive seismic tomography and laboratory experiments on rock samples, allow us to make some inferences about the location of the brittle–ductile transition, shallow aquifers, and the thermal–rheological state of rocks down to 5 km depth. Clear evidence for magma chambers only comes from petrological studies, indicating two main depth ranges for magma accumulation (5–8 and 11–15 km). As in most of the caldera areas, no clear seismological evidence exists for large volumes of low P-velocities, thus indicating that the residual magma chamber should rather be characterized by a high degree of crystallization, probably because of degassing.

While the models for the occurrence of unrest help to constrain possible pre-eruptive scenarios, indicating the additional complexity of eruption forecast at calderas, with respect to central volcanoes, the use of accurate modelling and statistical methodologies allow us to reconstruct, from detailed studies of past eruptive history, the probability of occurrence of the main destructive events linked to pyroclastic product emission in the whole Campi Flegrei and Neapolitan area.

The complex dynamics evidenced at Campi Flegrei, characterized by strict magma–water interaction not only during eruptions, and the problems linked to location and rheology of

magma chambers, all indicate the need for detailed, direct studies of caldera substructure by deep drilling. Detailed study of Campi Flegrei caldera, which represents a typical example of partially submerged super-volcano located in a densely populated urban area, thus gives a unique opportunity to deeply understand the dynamics of the most dangerous volcanoes on Earth, representing the most catastrophic natural hazards, after giant meteoritic impacts.

References

AGIP 1987. *Geologia e Geofisica del Sistema Geotermico dei Campi Flegrei*. Technical Report, SERG–ESG, San Donato, Italy.

APPLEYARD, S. 1995. The impact of urban development on recharge and groundwater quality in a coastal aquifer near Perth, Western Australia. *Hydrogeology Journal*, **3**, 65–75.

ARNET, F., KAHLE, H.-G., KLINGELE, E., SMITH, R. B., MEERTENS, C. M. & DZURISIN, D. 1997. Temporal gravity and height changes of Yellowstone caldera, 1977–1994. *Geophysical Research Letters*, **24**, 2741–2744.

ASTER, R. C. & MEYER, R. P. 1988. Three-dimensional velocity structure and hypocenter distribution in the Campi Flegrei caldera, Italy. *Tectonophysics*, **149**, 195–218.

ASTER, R. C., MEYER, R. P. *ET AL.* 1992. Seismic investigation of the Campi Flegrei: a summary and synthesis of results. *In:* GASPARINI, P., SCARPA, R. & AKI, K. (eds) *Volcanic Seismology.* Springer-Verlag, Berlin and Heidelberg, 462–483.

BABBAGE, C. 1847. *Observation on the Temple of Serapis at Pozzuoli Near Naples*. R. and J. E. Taylor, London.

BATTAGLIA, M., ROBERTS, C. & SEGALL, P. 2003. The mechanics of unrest at Long Valley caldera, California: 2. constraining the nature of the source using geodetic and micro-gravity data. *Journal of Volcanology and Geothermal Research*, **127**, 219–245.

BATTAGLIA, M., TROISE, C., OBRIZZO, F., PINGUE, F. & DE NATALE, G. 2006. Evidence for fluid migration as the source of deformation at Campi Flegrei caldera (Italy). *Geophysical Research Letters*, **33**, doi:10.1029/2005GL024904.

BEAUDUCEL, F., DE NATALE, G., OBRIZZO, F. & PINGUE, F. 2004. 3-D modelling of Campi Flegrei ground deformations: role of caldera boundary discontinuities. *Pure and Applied Geophysics*, **161**, doi:10.1007/s00024-004-2507-4.

BELLUCI, F., WOO, J., KILBURN, C. R. J. & ROLAND, G. 2006. Ground deformation at Campi Flegrei, Italy: implications for hazard assessment. *In*: TROISE, C., DE NATALE, G. & KILBURN, C. R. J. (eds) *Mechanisms of Activity and Unrest at Large Calderas.* Geological Society, London, Special Publications, **269**, 141–158.

BERRINO, G. 1994. Gravity changes induced by height-mass variations at the Campi Flegrei caldera. *Journal of Volcanology and Geothermal Research*, **61**, 293–309.

BERRINO, G. 1995. *Misure Distanziometriche ai Campi Flegrei – Giugno 1995.* Internal Report, Osservatorio Vesuviano, Naples.

BERRINO, G., CORRADO, G., LUONGO, G. & TORO, B. 1984. Ground deformation and gravity changes accompanying the Pozzuoli uplift. *Bulletin Volcanologique*, **47**, 187–200.

BIANCHI, R., CORADINI, A. *et al.* 1987. Modelling of surface ground deformation in volcanic areas: the 1970–1972 and 1982–1984 crises of Campi Flegrei, Italy. *Journal of Geophysical Research*, **92**, 14 139–14 150.

BIANCO, F., DEL PEZZO, E., SACCOROTTI, G. & VENTURA, G. 2004. The role of hydrothermal fluids in triggering the July–August 2000 seismic swarm at Campi Flegrei, Italy: evidence from seismological and mesostructural data. *Journal of Volcanology and Geothermal Research*, **133**, 229–246.

BONAFEDE, M. 1991. Hot fluid migration; an efficient source of ground deformation; application to the 1982–1985 crisis at Campi Flegrei – Italy. *Journal of Volcanology and Geothermal Research*, **48**, 187–198.

BONAFEDE, M., DRAGONI, M. & QUARENI, F. 1986. Displacement and stress fields produced by a centre of dilatation and by a pressure source in a viscoelastic half-space: application to the study of ground deformation and seismic activity at Campi Flegrei, Italy. *Geophysical Journal of the Royal Astronomical Society*, **87**, 455–485.

BREISLAK, S. 1792. *Essai Mineralogiques sur le Solfatare de Pouzzole; Part 3, Observations sur l'Exterieur du Cratere de la Solfatare.* Giaccio, Naples, 170–177.

BUROV, E. B. & GUILLOU-FROTTIER, L. 1999. Thermo-mechanical behavior of large ash flow calderas. *Journal of Geophysical Research*, **104**, 23 081–23 109.

CHIARABBA, C., AMATO, A. & DELANEY, P. T. 1997. Crustal structure, evolution, and volcanic unrest of the Alban Hills, Central Italy. *Bulletin of Volcanology*, **59**, 161–170.

CHIARABBA, C., AMATO, A., BOSCHI, E. & BARBERI, F. 2000. Recent seismicity and tomographic modelling of the Mount Etna plumbing system. *Journal of Geophysical Research*, **105**, 10 923–10 938.

CHIODINI, G., TODESCO, M., CALIRO, S., DEL GAUDIO, C., MACEDONIO, G. & RUSSO, M. 2003. Magma degassing as a trigger of bradyseismic events; the case of Phlegrean Fields, Italy. *Geophysical Research Letters*, **30**, 1434, doi:10.1029/2002GL016790.

CLARK, D. A., SAUL, S. J. & EMERSON, D. W. 1986. Magnetic and gravity anomalies of a triaxial ellipsoid. 1986. *Exploration Geophysics*, **17**, 189–200.

CONNOR, B. C., HILL, E. B., WINFREY, B., FRANKLIN, M. N. & LA FEMINA, C. P. 2001. Estimation of volcanic hazards from tephra fallout. *Natural Hazards Review*, **February**, 33–42.

De Gori, P., Cimini, G. B., Chiarabba, C., De Natale, G., Troise, C. & Deschamps, A. 2001. Teleseismic tomography of the Campanian volcanic area and surrounding Apennic belt. *Journal of Volcanology and Geothermal Research*, 1**09**, 52–75.

Deino, A. L., Orsi, G., de Vita, S. & Piochi, M. 2004. The age of the Neapolitan Yellow Tuff caldera forming eruption (Campi Flegrei caldera Italy) assessed by $^{40}Ar/^{39}Ar$ dating method. *Journal of Volcanology and Geothermal Research*, **133**, 157–170.

De Lorenzo, S., Zollo, A. & Mongelli, F. 2001. Source parameters and 3-D attenuation structure from the inversion of microearthquake pulse width data: Q_p imaging and inferences on the thermal state of the Campi Flegrei Caldera. *Journal of Geophysical Research*, **106**, 16 265–16 286.

De Natale, G. & Pingue, F. 1993. Ground deformations in collapsed caldera structures. *Journal of Volcanology and Geothermal Research*, **57**, 19–38.

De Natale, G. & Zollo, A. 1986. Statistical analysis and clustering features of the Phlegraean Fields earthquake sequence (May 1983–May 1984). *Bulletin of the Seismological Society of America*, **76**, 801–814.

De Natale, G., Pingue, F., Allard, P. & Zollo, A. 1991. Geophysical and geochemical modeling of the Campi Flegrei caldera. *Journal of Volcanology and Geothermal Research*, **48**, 199–222.

De Natale, G., Zollo, A., Ferraro, A. & Virieux, J. 1995. Accurate fault mechanism determinations for a 1984 earthquake swarm at Campi Flegrei caldera (Italy) during an unrest episode: implications for volcanological research. *Journal of Geophysical Research*, **100**, 24 167–24 185.

De Natale, G., Petrazzuoli, S. M. & Pingue, F. 1997. The effect of collapse structures on ground deformations in calderas. *Geophysical Research Letters*, **24**, 1555–1558.

De Natale, G., Troise, C. & Pingue, F. 2001. A mechanical fluid-dynamical model for ground movements at Campi Flegrei caldera. *Journal of Geodynamics*, **32**, 487–517.

De Natale, G., Troise, C., Trigila, R., Dolfi, D. & Chiarabba, C. 2004. Seismicity and 3D substructure at Somma-Vesuvius volcano: evidence for magma quenching. *Earth and Planetary Science Letters*, **221**, 181–196.

De Natale, G., Troise, C., Pingue, F., Mastrolorenzo, G. & Pappalardo, L. 2006. The Somma–Vesuvius volcano (Southern Italy): structure, dynamics and hazard evaluation. *Earth Science Reviews*, **74**, 73–111.

De Vivo, B., Rolandi, G., Gans, P. B., Calvert, A., Bohrson, W. A., Spera, F. J. & Belkin, H. E. 2001. New constraints on the pyroclastic eruptive history of the Campanian Volcanic Plain (Italy). *Mineralogy and Petrology*, **73**, 47–65.

Di Vito, M., Isaia, R., Orsi, G., Southon, J., D'Antonio, M., de Vita, S., Pappalardo, L. & Piochi, M. 1999. Volcanic and deformation history of the Campi Flegrei caldera in the past 12 ka. *Journal of Volcanology and Geothermal Research*, **91**, 221–246.

Del Gaudio, G., Ricco, C., Aquino, I., Brandi, G., Serio, C. & Siniscalchi, V. 2005. *Misure di livellazione di precisione e dati tiltmetrici per il controllo delle deformazioni del suolo ai Campi Flegrei*. Osservatorio Vesuviano, Naples, Open File Report No. 4.

Dragoni, M. & Magnanensi, C. 1989. Displacement and stress produced by a pressurized, spherical magma chamber, surrounded by a viscoelastic shell. *Physics of the Earth and Planetary Interiors*, **56**, 316–328.

Dvorak, J. J. & Berrino, G. 1991. Recent ground movement and seismicity activity in Campi Flegrei, Southern Italy: episodic growth of a resurgent dome. *Journal of Geophysical Research*, **96**, 2309–2323.

Dvorak, J. J. & Mastrolorenzo, G. 1991. The mechanism of recent vertical crustal movements in Campi Flegrei caldera, Southern Italy. *Geology Society of America*, *Special Paper*, **263**.

Eberhart-Phillips, D. & Michael, A. J. 1998. Seismotectonics of the Loma Prieta, California, region determined from three-dimensional V_P, V_P/V_s, and seismicity. *Journal of Geophysical Research*, **103**, 21 099–21 120.

Efron, B. & Tibshirani, R. 1986. Bootstrap methods for standard errors, confidence intervals, and other measures of statistical accuracy. *Statistical Science*, **1**, 54–77.

Eggers, A. 1987. Residual gravity changes and eruption magnitudes. *Journal of Volcanology and Geothermal Research*, **33**, 201–216.

Fialko, Y., Kazhan, Y. & Simons, M. (2001). Deformation due to a pressurized horizontal circular crack in an elastic half-space, with applications to volcano geodesy. *Geophysical Journal International*, **146**, 181–190.

Ferrucci, F., Hirn, A., Virieux, J., De Natale, G. & Mirabile, L. 1992. P-SV conversions at a shallow boundary beneath Campi Flegrei Caldera (Naples, Italy): evidence for the magma chamber. *Journal of Geophysical Research*, **97**, 15 351–15 359.

Fialko, Y., Kazhan, Y. & Simons, M. 2001. Deformation due to a pressurized horizontal circular crack in an elastic half-space, with applications to volcano geodesy. *Geophysical Journal International*, **146**, 181–190.

Forbes, J. D. 1829. Physical notice in the Bay of Naples; Number 5, on the Temple of Jupiter Serapis at Pozzuoli and the phenomena which it exhibits. *Edinburgh Journal of Science New Series*, **1**, 260–286.

Fournier, R. 1999. Hydrothermal processes related to movement of fluid from plastic into brittle rock in the magmatic epithermal environment. *Economic Geology*, **94**, 1193–1211.

Friedlander, S. K. 1977. *Smoke, Dust and Hazþ: Fundamentals of Aerosol Behaviour*, John Wiley, New York.

Gaeta, F. S., De Natale, G. *et al.* 1998. Genesis and evolution of unrest episodes at Campi Flegrei caldera: the role of the thermal fluid-dynamical processes in the geothermal system. *Journal of Geophysical Research*, **103**, 20 921–20 933.

GAETA, F. S., PELUSO, F., ARIENZO, I., CASTAGNOLO, D., DE NATALE, G., MILANO, G., ALBANESE, C. & MITA, D. G. 2003. A Physical appraisal of a new aspect of bradyseism: the miniuplifts. *Journal of Geophysical Research*, **108**, 20 921–20 933, doi:10.1029/2002JB001913.

GOTTSMANN, J., BERRINO, G., RYMER, H. & WILLIAMS-JONES, G. 2003. Hazard assessment during caldera unrest at the Campi Flegrei, Italy; a contribution from gravity–height gradients. *Earth and Planetary Science Letters*, **211**, 295–309.

GUNTHER, R. T. 1903. *The submerged Greek and Roman Foreshore near Naples*. Archaeologia, **58**, 499–560.

JUDENHERC, S. & ZOLLO, A. 2004. The Bay of Naples (southern Italy); constraints on the volcanic structures inferred from a dense seismic survey. *Journal of Geophysical Research*, **109**(B10).

KILBURN, C. R. J. & SAMMONDS, P. R. 2005. Maximum warning times for imminent volcanic eruptions. *Geophysical Research Letters*, **32**, L24313, doi:10.1029/2005 GL024184.

LAFEHR, T. R. 1991. Standardization in gravity reduction. *Geophysics*, **56**, 1170–1178.

LYELL, C. 1872. *Principles of Geology*. 11th edn., J. Murray, London, 164–179.

MCTIGUE, D. F. 1987. Elastic stress and deformation near a finite spherical, magma body: resolution of the point source paradox. *Journal of Geophysical Research*, **92**, 12 931–12 940.

MCEWEN, A. S. & MALIN, M. C. 1989. Dynamics of Mount St. Helens' 1980 pyroclastic flow, rockslide–avalanche, lahars, and blast. *Journal of Volcanology and Geothermal Research*, **37**, 205–231.

MACEDONIO, G. & TAMMARO, U. (eds) 2005. *Rendiconto sull' attività di sorveglianza anno 2003*. Osservatorio Vesuviano, Naples.

MASTROLORENZO, G., PAPPARLARDO, L., TROISE, C., ROSSANO, S., PANIZZA, A. & DE NATALE, G. 2006. Volcanic hazard assessment at Campi Flegrei Caldera. *In*: TROISE, C., DE NATALE, G. & KILBURN, C. R. J. (eds) *Mechanisms of Activity and Unrest at Large Calderas*. Geological Society, London, Special Publications, **269**, 159–172.

MOGI, K. 1958. Relations between the eruptions of various volcanoes and the deformations of the ground surfaces around them. *Bulletin of Earthquake Research*, **36**, 99–134.

MORHANGE, C., BOURCIERN, M., LABOREL, J., GIALLANELLA, C., GOIRAN, J. P., CRIMACO, L. & VECCHI, L. 1999. New data on historical relative sea level movements in Pozzuoli Phlaegrean Fields, Southern Italy. *Physics and Chemistry of the Earth*, **A24**, 349–354.

NAIRN, I. A., MCKEE, C. O., TALAI, B. & WOOD, C. P. 1995. Geology and eruptive history of the Rabaul Caldera area, Papua New Guinea. *Journal of Volcanology and Geothermal Research*, **69**, 255–284.

NERI, A., ESPOSTI ONGARO, T., MACEDONIO, G. & GIDASPOW, D. 2003. Multiparticle simulation of collapsing volcanic column and pyroclastic flows. *Journal of Geophysical Research*, **108**, doi: 10.1029/2001JB000508.

NICCOLINI, A. 1839. *Tavola Cronologica–metrica delle Varie Altezze Tracciate della Superficie del Mare fra la Costa di Amalfi ed il Promontorio di Gaeta nel Corso di Diciannove Secoli*. Flautina, Naples, 11–52.

NICCOLINI, A. 1845. *Descrizione della gran terma puteolana volgarmente detta Tempio di Serapide*. Stamperia Reale, Naples.

PAPPALARDO, L., CIVETTA, L. ET AL. 1999. Chemical and isotopical evolution of the Phlegraean magmatic system before the Campanian Ignimbrite (37 ka) and the Neapolitan Yellow Tuff (12 ka) eruptions. *Journal of Volcanology and Geothermal Research*, **91**, 141–166.

PAPPALARDO, L., PIOCHI, M., D'ANTONIO, M., CIVETTA, L. & PETRINI, R. 2002. Evidence for multi-stage magmatic evolution during the past 60 ka at Campi Flegrei (Italy) deduced from Sr, Nd and Pb isotope data. *Journal of Petrology*, **43**, 1415–1434.

PAPPALARDO, L., PIOCHI, M. & MASTROLORENZO, G. 2004. The 3800 yr BP–1944 AD magma plumbing system of Somma–Vesuvius: constraints on its behaviour and present state through a review of isotope data. *In*: DE NATALE, L. & DE VIVO (eds), *Annals of Geophysics*, **47**, 1471–1483.

PARASCANDOLA, A. 1947. *I Fenomeni Bradisismici del Serapeo di Pozzuoli*, Naples, privately published.

PRESTI, D., TROISE, C. & DE NATALE, G. 2004. Probabilistic location of seismic sequences in heterogeneous media. *Bulletin of the Seismological Society of America*, **94**, 2239–2253.

ROSI, M. & SBRANA, A. 1987. *Phlegraean Fields*. Quaderni de 'La Ricerca Scientifica', **114** CNR, Roma, 114–175.

ROSSANO, S., MASTROLORENZO G. & DE NATALE G. 2004. Numerical simulation of pyroclastic density currents on Campi Flegrei topography: a tool for statistical hazard estimation, *Journal of Volcanology and Geothermal Research*, **132**, 1–14.

SHERIDAN, M. F. 1979. Emplacement of pyroclastic flows: a review. *In*: CHAPIN & ELSTON (eds) *Ash Flow Tuffs*. Geological Society of America, Special Papers, **180**, 125–136.

SCHON, J. H. 2004. *Physical Properties of Rocks: Fundamentals and Principles of Petrophysics. Handbook of Geophysical Exploration and Seismic Exploration. In*: K. HELBIG, K. & TREITEL, S. (eds), Elsevier, Amsterdam.

SUZUKI, T. 1983. A theoretical model for dispersion of tephra. *In*: SHIMOZURU, D. & YOKOYAMA, I. (eds) *Arc Volcanism: Physics and Tectonics*, Terra Scientific Publishing Company (Terrapub), Tokyo, 95–113.

THURBER, C. H. 1993. Local earthquake tomography: velocities and V_p/V_s – theory. *In*: IYER, H. M. & HIRAHARA, K. (eds) *Seismic Tomography*, Chapman & Hall, London.

TRASATTI, E., GIUNCHI, C. & BONAFEDE, M. 2005. Structural and rheological constraints on source depth and overpressure estimates at Campi Flegrei Caldera, Italy. *Journal of Volcanology and Geothermal Research*, **144**, 105–118.

TROISE, C., DE NATALE, G., PINGUE, F. & ZOLLO, A. 1997. A model for earthquake generation during unrest crises at Campi Flegrei and Rabaul calderas. *Geophysical Research Letters*, **24**, 1575–1578.

TROISE, C., CASTAGNOLO, D., PELUSO, F., GAETA, F. S., MASTROLORENZO, G. & DE NATALE, G. 2001. A 2D mechanical–thermal fluid-dynamical model for geothermal systems at calderas: an application to Campi Flegrei, Italy. *Journal of Volcanology and Geothermal Research*, **109**, 1–12.

TROISE, C., PINGUE, F. & DE NATALE, G. 2003. Coulomb stress changes at calderas: modeling the seismicity of Campi Flegrei (Southern Italy). *Journal of Geophysical Research*, **108**, doi:10.1029/2002JB002006.

TROISE, C., DE NATALE, G. & PINGUE, F. 2004. Non linear effects in ground deformation at calderas due to the presence of structural discontinuities. *Annals of Geophysics*, **47**, 1513–1520.

VANORIO, T., VIRIEUX, J., CAPUANO, P. & RUSSO, G. 2005. Three dimensional seismic tomography from P wave and S wave microearthquake travel times and rock physics characterization of the Campi Flegrei caldera. *Journal of Geophysical Research*, **110**, doi:10.1029/2004JB003102.

VINCIGUERRA, S., TROVATO, C., MEREDITH, P. G., BENSON, P. M., DE LUCA, G., TROISE, C. & G. DE NATALE, 2006. Understanding the seismic velocity structure of Campi Flegrei caldera (Italy): from the laboratory to the field scale. *Pure and Applied Geophysics*, in press.

WAITE, G. R. & SMITH, R. B. 2002. Seismic evidence for fluid migration accompanying subsidence of the Yellowstone Caldera. *Journal of Geophysical Research*, **107**, 10.1029/2001JB000586.

WALSH, J. & RICE, J. 1979. Local changes in gravity resulting from deformation. *Journal of Geophysical Research*, **84**, 165–170.

WEILAND, C. M., STECK, L. K., DAWSON, P. B. & KORNEEV, V. A. 1995. Non-linear teleseismic tomography at Long Valley caldera, using three-dimensional minimum travel time ray tracing. *Journal of Geophysical Research*, **100**, 20 379–20 390.

XU, Y. & VAN TONDER, G. J. 2001. Estimation of recharge using a revised CRD method. *Water South Africa*, **27**, 341–343.

YANG, X., DAVIS, P. M. & DIETERICH, J. H. 1988. Deformation from inflation of a dipping finite prolate spheroid in an elastic half-space as a model for volcanic stressing. *Journal of Geophysical Research*, **93**, 4249–4257.

ZAMORA, M., SARTORIS, G. & CHELINI, W. 2001. Laboratory measurements of ultrasonic wave velocities in rocks from the Campi Flegrei volcanic system and their relation to other field data. *Journal of Geophysical Research*, **99**, 13 553–13 562, doi:10.1029/94JB00121, 2163–2166.

ZOLLO, A., JUDENHERC, S. *ET AL.* 2003. Evidence for the buried rim of Campi Flegrei caldera from 3-D active seismic imaging. *Geophysical. Research Letters*, **30**, doi:10.1029/2003GL018173.

ZOLLO, A., GASPARINI, P. *ET AL.* 1996. Seismic evidence for low velocity zone in the upper crust beneath Mount Vesuvius. *Science*, **274**, 592–594.